Journal of *Marine Science and Engineering*

MDPI

Article

Sr and Nd Isotopes in Mineral Fractions of Ferromanganese Crusts from the Northernmost Pacific

Pavel Mikhailik [1,*], Irina Vishnevskaya [1,2], Liang Yi [3], Natalia Soloshenko [4] and Vadim Pellinen [5]

[1] Far East Geological Institute, FEB RAS, Vladivostok 690022, Russia; vishnevskaia.i.a@gmail.com
[2] Vernadsky Institute of Geochemistry and Analytical Chemistry, RAS, Moscow 119334, Russia
[3] State Key Laboratory of Marine Geology, Tongji University, Shanghai 200092, China; yiliang@tongji.edu.cn
[4] Zavaritsky Institute of Geology and Geochemistry, UB RAS, Ekaterinburg 620010, Russia; nats_igg@mail.ru
[5] Institute of the Earth's Crust, SB RAS, Irkutsk 644033, Russia; vadim.a.pellinen@ya.ru
* Correspondence: mikhailik@fegi.ru

Abstract: A study of the isotopic compositions of neodymium and strontium in four mineral fractions of the hydrogenous ferromanganese crusts of the northernmost Pacific has been carried out for the first time. The relationship of the $^{87}Sr/^{86}Sr$ ratio and ε_{Nd} value of the residual fraction in heterochronous layers of the ferromanganese crusts have shown that the sources of detrital matter are from rock weathering by the Yukon River, the Kuskokwim River, the Anadyr River and the rivers of Kamchatka. The amount of aluminosilicate impurity does not affect the isotopic compositions of the chemogenic (loosely bound, Mn oxides or manganese, hydrous Fe oxides or ferrous) fractions. The decreased ε_{Nd} value in the ferrous fraction seems to be related to the presence of rare earth element (REE) phosphate complexes in seawater. The increase in those complexes is a consequence of melt waters entering the ocean during warming periods. Our data indicate that the carbonate REE complexes are not the dominant form of the REEs in the northernmost Pacific, which leads to the fact that the neodymium isotopic compositions of the manganese and ferrous fractions of hydrogenous ferromanganese crusts are different. A decrease in ε_{Nd} value in the ferrous fraction may be a marker of a local increase in the surface water bioproductivity. Our data also show that the increase of the REE in the ferrous fraction relative to the manganese fraction does not reflect the participation of hydrothermal matter in the formation of mixed hydrogenous–hydrothermal crusts but is a consequence of an increase in the REE phosphate complexes.

Keywords: ferromanganese crusts; mineral fractions; Sr and Nd isotopes; REE complexes; northernmost Pacific

check for updates

Citation: Mikhailik, P.; Vishnevskaya, I.; Yi, L.; Soloshenko, N.; Pellinen, V. Sr and Nd Isotopes in Mineral Fractions of Ferromanganese Crusts from the Northernmost Pacific. *J. Mar. Sci. Eng.* **2023**, *11*, 1920. https://doi.org/10.3390/jmse11101920

Received: 23 August 2023
Revised: 24 September 2023
Accepted: 25 September 2023
Published: 5 October 2023

Copyright: © 2023 by the authors. Licensee MDPI, Basel, Switzerland. This article is an open access article distributed under the terms and conditions of the Creative Commons Attribution (CC BY) license (https://creativecommons.org/licenses/by/4.0/).

1. Introduction

Ferromanganese deposits (crusts, nodules, etc.) developed on sea floors are marine sources for strategic metals, such as Mn, Co, and rare earth element (REE), and informative proxies recording oceanic paleoenvironment changes, e.g., [1–3]. These ferromanganese crusts usually grow on slopes and/or sediment-free seamounts/guyots, with a water depth range of 400 to 7000 m [1,4,5]. There are two types of ferromanganese crusts widespread on the seafloor, i.e., hydrogenous and hydrothermal [6]. For hydrogenous ones, metals are mainly from ambient seawater, while for hydrothermal ones, hydrothermal fluids are the main source [7]. For different geneses, mineralogical, geochemical and isotopic properties of ferromanganese crust are distinct, e.g., [8,9].

During the period of growth that spans millions of years, e.g., [10], hydrogenous crusts absorb dissolved metals from the seawater, and studying REEs and metal isotopes makes it possible to reconstruct water masses [11–15]. In addition, volcanic activities, aeolian input, and cosmogenic matter also have fingerprints in the growth processes of these crusts [16,17], and metal/mineral changes can be correlated with the glacial–interglacial alternations [18–22]. For example, most REEs in hydrothermal crusts are associated with

hydrous Fe oxides [23,24], while in hydrogenous crusts, REEs may be influenced by the competition between manganese and ferrous fractions [23,25].

Studying Sr and Nd isotopic composition of ferromanganese deposits helps to identify metal sources, reconstruct formation processes, and establish age models, e.g., [17,26,27]. Although the behavior of Sr and Nd isotopes in bulk ferromanganese crusts has been broadly studied [8,9,12,13,28,29], the balance of ε_{Nd} values and the $^{87}Sr/^{86}Sr$ ratios in different mineral fractions of ferromanganese deposits are not well known. To address this question, we have examined a collection of ferromanganese crust samples from the northernmost Pacific Ocean.

2. Materials and Methods

2.1. Study Area

The study area is not far from the continent, from aeolian source regions, and from active volcanic fields (Figure 1), allowing us to trace how profound the terrigenous influence is in the neodymium and strontium isotopic compositions in mineral fractions of ferromanganese crusts.

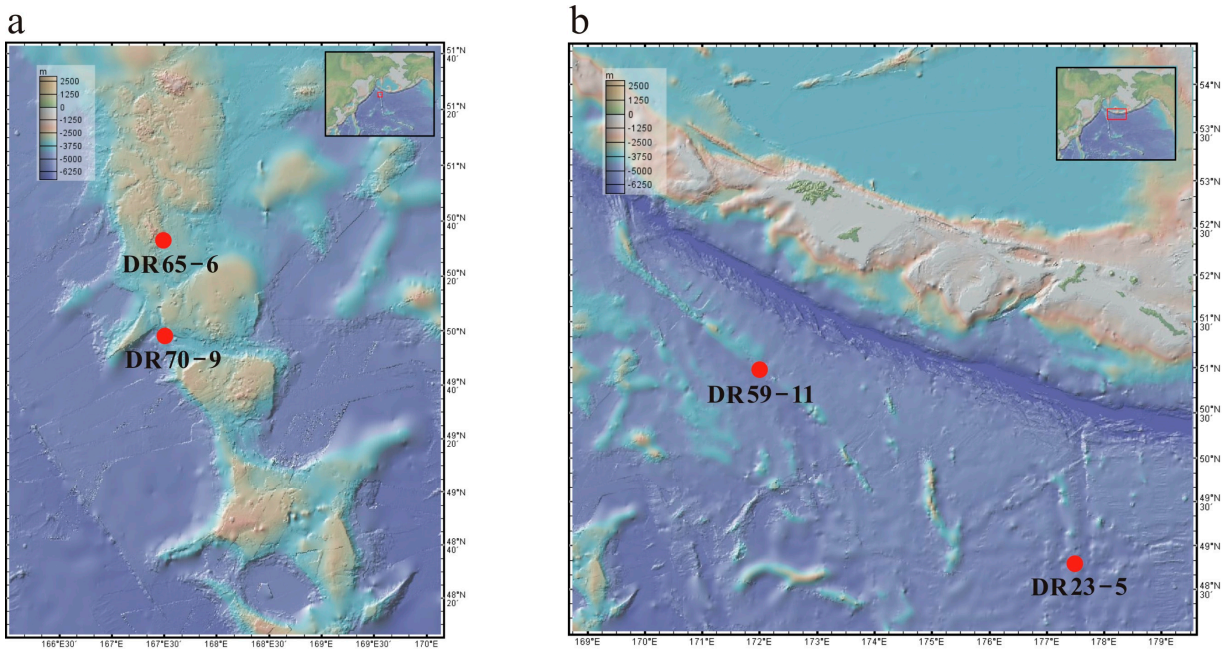

Figure 1. Location of the study area and crust sites. (**a**) The Hanzei and Detroit Guyots in the Emperor Ridge; (**b**) The Rat and Stalemate Fracture Zones.

The Hanzei and Detroit Guyots are parts of the northern segment of the Emperor Ridge, which extends southward for 2300 km to the Hawaiian hotspot [30]. These guyots are flat-topped seamounts that represent an earlier stage of the Hawaiian hotspot (~80–60 Ma). The age of the Detroit Guyot is about 82–76 Ma [31–33], while the Hanzei Guyot is thought to be older than 73 Ma [34]. The Rat Fracture Zone (FZ) extends in a S-N direction and intersects the Aleutian Trench at nearly a right angle. The Stalemate FZ has a strike that is oriented north-west. Around 169°45′ E, the Stalemate FZ bends in a north-north-west direction and gradually into the trench [35].

2.2. Studied Crusts

The studied ferromanganese crusts (Figure 2) were collected from the slopes of the Hanzei and Detroit Guyots in the Emperor Ridge (Figure 1a) and from the Rat and Stalemate FZs (Figure 1b), during the scientific expedition of the R/V Sonne (249th cruise, 2016). All of the studied crusts (Figure 2) are hydrogenous, based on mineral composition and metal ratios [36], and analysis of bulk samples indicates the following elemental

contents (Table 1): Si (13.0 ± 5.1%), Al (2.7 ± 1.3%), Ca (1.9 ± 0.2%), Fe (19.1 ± 3.8%), Mn (13.3 ± 5.7%), Co (1300 ± 591 ppm), Cu (850 ± 816 ppm), and Ni (1644 ± 1298 ppm).

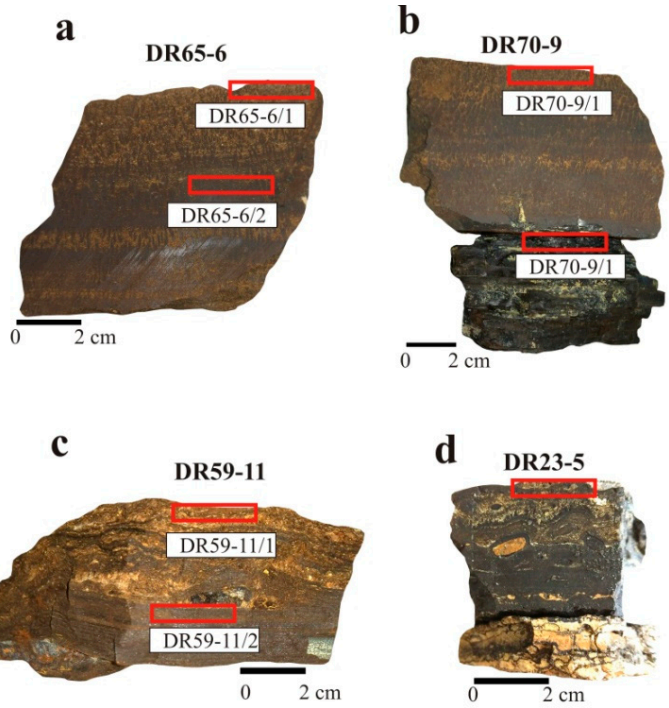

Figure 2. The studied sections of ferromanganese crust in this work. (**a**) Fe-Mn crust from the Detrioit Guyot; (**b**) Fe-Mn crust from the Hanzei Guyot; (**c**) Fe-Mn crust from the Stalemate FZ; (**d**) Fe-Mn crust from the Rat FZ.

Table 1. The information on the studied crusts.

No.	Sampling Position	Latitude, N	Longitude, W	Water Depth, m	Structure	Minerals [(a)]
			Fracture Zones			
DR23-5	0–2 mm	48°44′17″	177°30′14″	5088–4510	Rat	Vernadite, 10 Å Manganate
DR59-11/1	0–2 mm	51°1′26″	172°1′19″	4274–3814	Stalemate	Quartz, Plagioclase, Vernadite (?)
DR59-11/2	31–36 mm					Vernadite
			Emperor Guyots			
DR65-6/1	0–2 mm	50°31′59″	167°28′59″	3313–2897	Detroit	Vernadite
DR65-6/2	20–25 mm					Vernadite
DR70-9/1	0–2 mm	50°1′1″	167°30′32″	3685–3278	Hanzei	Vernadite
DR70-9/2	60–65 mm					Vernadite

Note: [(a)] Mineral data were from [36] (?)—probably.

In the ternary diagram based on Mn-Fe-(Co+Cu+Ni) × 10 [6], part of the samples are located in the hydrothermal area or on the border between two genetic types (Figure 3). As is known, hydrothermal ferromanganese deposits composed of bernessite, todorokite or pyrolusite [7] and hydrogenic crusts contain vernadite [4]. Vernadite in hydrothermal deposits likely indicates a high growth rate and, as a consequence, low concentrations of Co, Cu and Ni are observed (Table 2), relative to typical hydrogenetic Co-rich crusts [37].

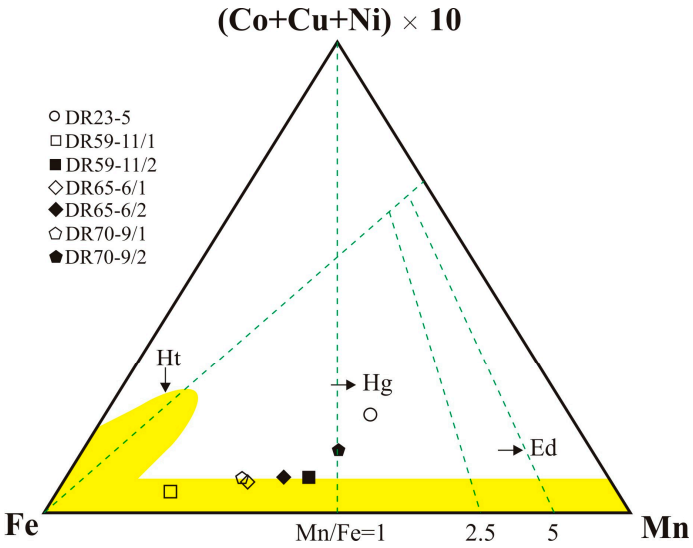

Figure 3. Ternary diagram of Fe, Mn, and (Co+Cu+Ni) × 10, following [6]. The yellow-shaded area indicates the main influence of hydrothermal (Ht) processes; Hg, hydrogenetic; Ed, early diagenetic.

Table 2. Chemical composition of bulk samples of the studied crusts.

Element	DR65-6/1	DR65-6/2	DR70-9/1	DR70-9/2	DR23-5	DR59-11/1	DR59-11/2
Mn (%)	10.2	15.0	10.3	21.8	15.8	4.06	16.2
Fe (%)	20.2	22.5	21.2	21.5	11.8	16.2	20.0
Ca (%)	1.70	1.85	1.77	2.15	2.23	2.07	1.84
Si (%)	14.3	9.81	13.6	5.32	15.5	21.5	10.8
Al (%)	2.95	1.87	2.82	0.87	3.82	4.63	2.02
Co (ppm)	1198	1291	1278	2490	1172	500	1176
Ni (ppm)	744	1582	799	3254	3607	226	1297
Cu (ppm)	351	472	498	1109	2596	284	637
Sr (ppm)	1075	1334	1084	1707	833	659	1200
Y (ppm)	152	213	154	225	90.1	67.2	196
La (ppm)	237	347	249	408	132	125	317
Ce (ppm)	780	1131	890	1841	958	397	930
Pr (ppm)	55.0	77.0	59.9	111	38.0	31.9	78.4
Nd (ppm)	224	315	240	400	149	129	315
Sm (ppm)	52.3	71.0	55.0	93.9	39.1	29.9	74.7
Eu (ppm)	13.2	18.0	12.6	20.9	9.58	7.34	18.5
Gd (ppm)	58.2	78.0	54.3	88.7	38.1	30.1	79.3
Tb (ppm)	8.12	11.5	8.33	14.0	5.83	4.34	11.6
Dy (ppm)	44.3	62.8	44.8	73.1	30.8	22.6	62.3
Ho (ppm)	8.14	11.8	8.25	13.5	5.35	3.95	11.5
Er (ppm)	22.3	32.5	22.2	36.9	14.7	10.5	31.0
Tm (ppm)	3.07	4.47	3.06	5.27	2.11	1.42	4.28
Yb (ppm)	19.4	28.6	19.4	32.7	13.0	9.25	27.1
Lu (ppm)	2.82	4.09	2.81	4.79	1.87	1.32	3.90
∑REE (ppm)	1529	2193	1670	3147	1439	804	1965
Ce/Ce*	1.57	1.59	1.68	1.98	3.10	1.44	1.36
Eu/Eu*	1.11	1.13	1.08	1.08	1.16	1.15	1.13
ε_{Nd}	−3.3 ± 0.1	−3.2 ± 0.1	−3.3 ± 0.1	−4.4 ± 0.1	−3.2 ± 0.2	−2.3 ± 0.2	−3.3 ± 0.1
$^{87}Sr/^{86}Sr$	0.708780 ± 0.000006	0.709110 ± 0.000004	0.709047 ± 0.000007	0.709141 ± 0.000008	0.708563 ± 0.000010	0.707973 ± 0.000005	0.709021 ± 0.000010

Note: Element concentration, ε_{Nd} value and $^{87}Sr/^{86}Sr$ ratio data were from [9,36].

For this study, seven samples (Figure 2) from each of four crusts were collected (Table 1). For each sample, the bulk sample and four subsamples in different mineral

fractions, namely loosely bound (I or carbonate), Mn oxide (II), hydrous Fe oxide (III), and residual (IV or silicate), were prepared for later measurements.

The maximum ∑REE (3147 ppm) is found in sample DR70-9/2, in which Cerium is 1841 ppm (Table 2). For the remaining crusts, this value varies between 804–2193 ppm (Table 2). All samples are characterized by a positive Ce anomaly ($Ce/Ce^* = Ce_{sn}/(La_{sn} \times 0.5 + Pr_{sn} \times 0.5)$; the index "sn" is normalized by the Post-Archean Australian shale (PAAS) [38], which varies from 1.36 to 3.10 (Figure 4, Table 2). Its maximum value is found in the FZ Rat sample (DR23-5), where Cerium is 958 ppm. The Eu anomaly ($Eu/Eu^* = Eu_{sn}/(Sm_{sn} \times 0.5 + Gd_{sn} \times 0.5)$) values are also positive, with a narrower range of 1.08–1.16 (Table 2). The REE patterns (Figure 4a) are similar to those of hydrogenetic deposits [39]. Moreover, in the discrimination diagrams, the samples are located in a hydrogenetic area (Figure 4b,c).

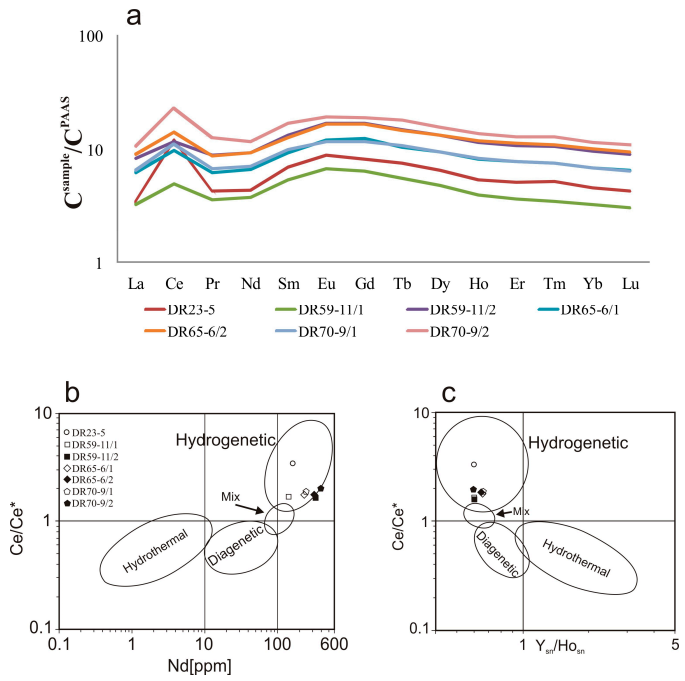

Figure 4. Shale-normalized REE distribution patterns of ferromanganese crusts (**a**) and sample location in graphs of (**b**) Ce/Ce* ratio vs. Nd concentration and (**c**) Ce/Ce* ratio vs. Y_{sn}/Ho_{sn} ratio.

2.3. Measurements

The bulk chemical analysis was made in the Collective Use Center (CUC) of the Far East Geological Institute, Far East Branch of the Russian Academy of Science. In the course of the elemental analysis by plasma spectrometry (ICP-AES and ICP-MS), the samples were dried to a constant weight at 105 C°. A weighed portion of the dried test sample (0.03 g) was placed in a platinum dish; a mixture of concentrated acids (HF, HNO_3, $HClO_4$) was added in a ratio of 3:5:1 and evaporated to wet salts; the treatment was repeated with HNO_3 and $HClO_4$ acid in a ratio of 1:0.5 and evaporated to wet salts again. Then, the samples were sequentially treated with deionized water and concentrated HNO_3, each time evaporating to wet salts. During the sample preparation, a Mn (IV) oxide precipitate was released from the samples. To restore it and convert it into a soluble form, treatment with 1–2 mL of 30% H_2O_2 and 10 mL of 26% HNO_3 was performed with heating. Then, the sample solution was transferred into 50 mL polypropylene volumetric flasks and filled up to the mark with deionized water. Aliquots of 10 mL for ICP-AES and 2 mL for ICP-MS were taken from the resulting solutions. Before performing ICP-MS measurements, the solutions were diluted 5 times.

The concentrations of Mn, Fe, Ca, and Al were determined using the multielement method of inductively coupled plasma atomic emission spectrometry (ICP-AES) on an

iCAP 7600 Duo spectrometer (Thermo Scientific, Waltham, MA, USA). In this case, the Si content in the sample was determined by the classical gravimetric method from a weighed portion of 0.1 g after fusing the powder sample with anhydrous sodium carbonate.

The trace element composition of the samples (Co, Ni, Cu, Sr, REE) was studied by inductively coupled plasma mass spectrometry (ICP-MS) using an Agilent 7700 spectrometer (Agilent Tech., Tokyo, Japan).

The pretreatment and measuring of Sr and Nd contents in mineral fractions are adapted from the procedures proposed by [40] and the details are listed in [9].

Our scheme of phase analysis comprises four fractions of successive sample treatment.

Fraction I. Treatment of 1 g sample with acetate buffer (1N CH_3COOH + 1N $CH_3COONa \cdot 3H_2O$, pH = 5) for 5 h at room temperature, with the sample: reagent proportion of 1:50 (w/w). This procedure leads to the extraction of calcium carbonate and associated elements and the release of absorbed ions. The obtained solution was filtered off. The filtrate was mineralized with concentrated HNO_3 in a microwave oven and was analyzed by ICP AES and ICP MS. The residue was washed with deionized type I water, dried, and subjected to the following treatment.

Fraction II. Extraction of Mn and associated elements by treatment of the residue with 0.5 M NH_2OH (pH = 2) for 3 min at room temperature, with the residue:reagent proportion of 1:100 (w/w). The obtained solutions were filtered off, hydroxylamine in the filtrate was decomposed by concentrated HNO_3 on heating, the solution was evaporated, and the precipitate was dissolved in 5% HNO_3. The solutions were analyzed by ICP AES and ICP MS.

Fraction III. The weighed portion of the dried residue was treated with a mixture of 0.2 M oxalic acid and ammonium oxalate (pH = 3.5, residue:solution proportion of 1:175 (w/w)) for 12 h at room temperature. The filtrate was evaporated to a wet salt and treated with concentrated HNO_3 to destroy the organic matrix. After evaporation, the residue was dissolved in 5% HNO_3. The resulting solutions were analyzed by ICP AES and ICP MS. These extracts contained Fe hydroxides.

Fraction IV. The solid residue obtained in the previous chemical treatment (an aluminosilicate fraction) was ashed together with the filter at 600 °C in a muffle furnace. Then, it was dissolved in a mixture of HF, HNO_3, and $HClO_4$ in a Teflon weighing bottle on heating. The obtained solutions were analyzed by ICP AES and ICP MS.

The isotopic composition of Sr and Nd (35 measurements in total) was conducted in the CUC "Geoanalitik" of the Institute of Geology and Geochemistry, the Ural Branch of the Russian Academy of Sciences (UB RAS) (Ekaterinburg). The portion of the dry substance of each fraction was dissolved in 0.5 mL of 7 M HNO_3 and centrifuged for 15 min at 6000 rpm (EBA 21 centrifuge, Hettich, Germany). The resulting solution was applied to the Sr resin column (100–200 mesh, Triskem). Sr was extracted by the stepwise elution technique in 7 M and 0.05 M HNO_3. The eluate was evaporated to wet salts and dissolved in 5 mL of 0.5% HNO_3. This solution was used to measure the $^{87}Sr/^{86}Sr$ ratio. The Sr isotopic composition was analyzed using a multi-collector inductively coupled mass spectrometer (Neptune Plus, Thermo Scientific). The correctness of the measurement technique was assessed using the international standard Sr SRM-987 ($^{87}Sr/^{86}Sr$ ratio during the period of operation was 0.710256 ± 0.000017, 2σ, n = 21). The mass fractionation was corrected by normalizing exponentially with an $^{88}Sr/^{86}Sr$ ratio of 8.3752.

For Nd isotopic composition, the procedure was carried out following [8]. The correctness of the measurement technique was assessed using the international standard JNdi-1 ($^{143}Nd/^{144}Nd$ ratio in the standard during the operation was 0.512107 ± 0.000010, 2σ, n = 15). The measurement error of the Nd isotopic composition was 0.005%.

For young samples (<10 Ma), the following equation for calculating ε_{Nd} used in this study is as follows:

$$\varepsilon_{Nd}(0) = \left(\frac{\left(\frac{^{143}Nd}{^{144}Nd}\right)}{\left(\frac{^{143}Nd}{^{144}Nd}\right)_{CHUR}} - 1 \right) \cdot 10{,}000$$

where $^{143}Nd/^{144}Nd$ is the Nd isotopic composition in the natural sample, and $(^{143}Nd/^{144}Nd)_{CHUR}$ is from the "homogeneous chondrite reservoir" with a value of 0.512638 [41].

3. Results

3.1. Sr and Nd in Bulk Samples

The Sr content varies substantially, from 659 ppm to 1707 ppm, and the obtained $^{87}Sr/^{86}Sr$ ratio of bulk samples ranges from 0.707973 to 0.709141 (Table 2). We also observe a significant correlation between Sr content and $^{87}Sr/^{86}Sr$ ratio ($r = 0.84$, $p < 0.01$, $n = 7$). In addition, the $^{87}Sr/^{86}Sr$ ratio of sample DR59-11/1 (0.707973 ± 0.000005) shifts to the values of typical volcanic rocks, implying a large number of quartz-plagioclase inputs during the crustal growth (Table 1).

The Nd isotopic composition, in terms of ε_{Nd}, ranges from -2.3 to -4.4 (Table 2), corresponding to isotopic compositions of North Pacific deep water [42]. The ε_{Nd} value of -2.3 is found in the sample with the maximum amount of allothigenous contamination, which is similar to previous estimates in the Detroit Guyot (-2.2 ± 0.1) [28]. The minimum value of ε_{Nd} (-4.4) is found in the ferromanganese crust of the Hanzei Guyot, where Al and Si inputs are limited. This value of ε_{Nd} (-4.4) can be correlated to values of the Miocene deep water in the northernmost Pacific [43].

3.2. Sr and Nd in Mineral Fractions

Sr and Nd isotopic compositions in mineral fractions are shown in Figure 5, and the difference between various fractions is evident. For sample DR65-6/1, the $^{87}Sr/^{86}Sr$ ratio in loosely bound (I), Mn oxide (II), and hydrous Fe oxide (III) are similar, i.e., 0.709182, 0.709188, and 0.709083, respectively, while the $^{87}Sr/^{86}Sr$ ratio in residual (IV) is different to others, that is, 0.706693. The difference between the four fractions is consistent with previous studies [44], confirming an exchange and equilibration of strontium isotopic composition in the marine ferromanganese deposits [45]. In contrast, ε_{Nd} changes have a large variance among various fractions. The change pattern of the $^{87}Sr/^{86}Sr$ ratio and ε_{Nd} values in samples DR65-6/2, DR70-90/1, DR70-90/2, and DR59-11/2 is similar to that of sample DR65-6/1 (Table 3). However, the $^{87}Sr/^{86}Sr$ ratio in samples DR59-11/1 and DR23-5 displays a large variance among various mineral fractions: $^{87}Sr/^{86}Sr$ ratios in loosely bound (I) and Mn oxide (II) are similar, while the $^{87}Sr/^{86}Sr$ ratios of hydrous Fe oxide (III) and silicate (IV) are significantly low (Figure 5e,g).

Table 3. ε_{Nd} and $^{87}Sr/^{86}Sr$ ratio in mineral fractions.

	DR65-6/1				DR65-6/2			
(a)	I	II	III	IV	I	II	III	IV
ε_{Nd}	−3.0	−3.7	−4.8	−3.6	−3.2	−3.2	−3.3	−2.2
±σ	0.2	0.3	0.4	0.1	0.1	0.1	0.1	0.2
$^{87}Sr/^{86}Sr$	0.709182	0.709188	0.709083	0.706693	0.709204	0.709173	0.708891	0.705495
±σ	0.000006	0.000007	0.000009	0.000012	0.000011	0.000006	0.000008	0.000007
	DR70-9/1				DR70-9/2			
(a)	I	II	III	IV	I	II	III	IV
ε_{Nd}	−3.6	−3.8	−3.0	−3.7	−4.2	−4.2	−4.5	−4.1
±σ	0.1	0.2	0.3	0.1	0.1	0.1	0.3	0.1
$^{87}Sr/^{86}Sr$	0.709196	0.709186	0.709167	0.706106	0.709183	0.709188	0.708961	0.706727
±σ	0.000009	0.000007	0.000008	0.000006	0.000006	0.000010	0.000012	0.000017

Table 3. *Cont.*

	DR59-11/1				DR59-11/2			
[(a)]	I	II	III	IV	I	II	III	IV
ε_{Nd}	−4.4	−3.0	−4.7	−1.8	−3.0	−3.4	−1.9	−2.9
±σ	0.3	0.2	0.5	0.1	0.2	0.2	1.5	0.3
$^{87}Sr/^{86}Sr$	0.709184	0.709197	0.708908	0.704898	0.709210	0.709161	0.709115	0.705741
±σ	0.000007	0.000008	0.000018	0.000008	0.000012	0.000019	0.000003	0.000009
	DR23-5							
[(a)]	I	II	III	IV				
ε_{Nd}	−3.6	−3.4	−3.4	−3.0				
±σ	0.4	0.2	0.3	0.3				
$^{87}Sr/^{86}Sr$	0.709195	0.709178	0.708978	0.706433				
±σ	0.000006	0.000008	0.000013	0.000005				

Note: [(a)] loosely bound (I), Mn oxide (II), Fe oxide (III), and residual (IV).

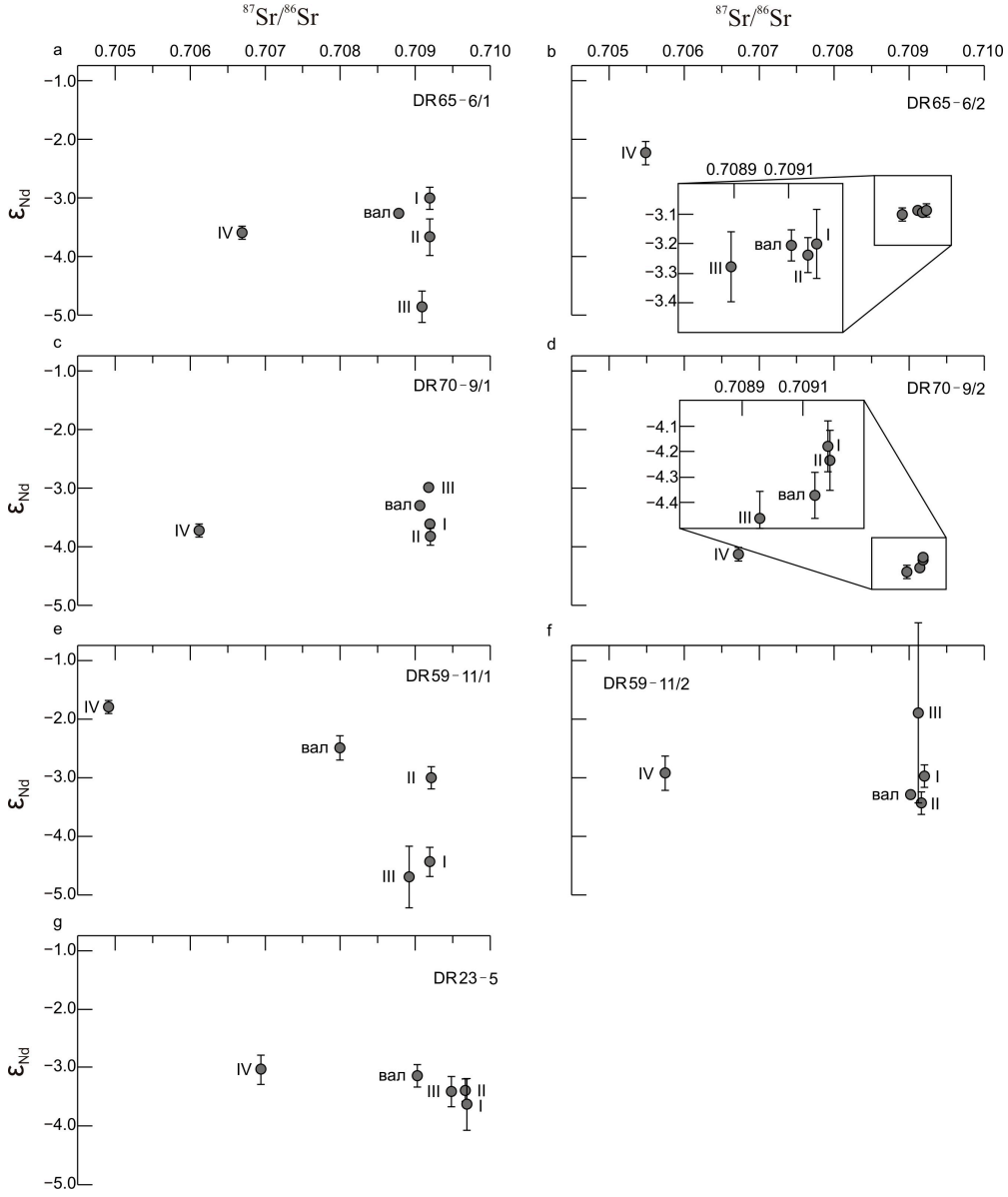

Figure 5. Sr and Nd isotopic compositions in mineral fractions of the studied crusts. (**a**,**b**) Fe-Mn crust from the Detrioit Guyot; (**c**,**d**) Fe-Mn crust from the Hanzei Guyot; (**e**,**f**) Fe-Mn crust from the Stalemate FZ; (**g**) Fe-Mn crust from the Rat FZ.

4. Discussion

Strontium isotopic composition is a valuable tool for age determination of deep-sea deposits, named as the Sr isotope stratigraphy, e.g., [45,46]. Our study has found that $^{87}Sr/^{86}Sr$ ratios of chemogenic fractions (I–III) are similar in different samples, against with that $^{87}Sr/^{86}Sr$ ratio in the samples with different ages should be distinct [44]. Thus, our $^{87}Sr/^{86}Sr$ results confirm a previous suggestion that the exchange and equilibration of strontium isotopic composition in the marine ferromanganese deposits may result in a failure in the Sr isotope stratigraphy [45].

Moreover, mineral fractions are known to exhibit different patterns of chemical elements in ferromanganese deposits [36,40], including REEs [23,25,47–49], which suggests that all chemogenic fractions record isotopic equilibrium [26,50]. In our study, similar ε_{Nd} values in samples DR23-5 and DR70-9/1 support this inference in surficial layers. A similar result is also observed in sample DR70-9/2, implying a unifying mechanism for the precipitation of the neodymium isotopic compositions over the depositing period.

However, it is found that for the samples taken from the surface layers (0–2 mm) of the Detroit Guyot (DR65-6/1) and the Stalemate FZ (DR59-11/1), the ε_{Nd} values in the Fe oxide fraction are persistently lower by 1.2–1.7 epsilon units, compared to the Mn oxide fraction. This discrepancy suggests that the isotopic equilibrium may have been disrupted in these samples.

During warm periods, the melting of glaciers could significantly increase detrital inputs, such as eolian dust, river sand, and glacial rubble, resulting in a more negative ε_{Nd} [20]. In addition, chemical weathering was induced during warm periods, leading to an increase in dissolved elements [51], which also contributes to a local negative in ε_{Nd} values. Thawing waters are found to be enriched with carbon and phosphate ions $(PO_4)^{3-}$ due to excessive productivity [52]. The increased supply of nutrient-rich freshwater from ice melt waters may induce the development of highly productive zones, reorganizing the distribution and species of microfauna, primarily diatoms and radiolarians [53–55]. The effect was evident during the Bølling–Allerød warming period (14,690–12,890 ka) in the Underwater Shirshov Ridge (the Bering Sea) and the Kamchatka Peninsula [55], and thus might be similar during the depositional period of the studied crusts.

It has been demonstrated that Nd tends to change with phosphate ions [56,57], and with phosphorus-associating Fe oxides [36,40,58]. Moreover, REEs in a water column gradually increase from the surface to the bottom, which is similar to the characteristics of nutrients such as phosphate. REEs can be enriched by coprecipitation with Fe-Mn oxide and phosphate, which is higher in the latter [27].

Phosphate ion acts as a complex-forming medium which increases in river, lake, and subsurface waters [59,60]. Melt waters lead to a decrease in dissolved REEs [59], indicating their complexation with phosphate ions. Thawing waters carrying REE phosphates with low ε_{Nd} values may thus contribute to crust formation. Consequently, the positively charged Fe oxide fraction (III) not only sorbs carbonate complex $(Nd(CO_3)^{2-})$, which is the main form of Nd in seawater [61], but also phosphate complexes of Nd in the form of $NdPO_4^0$. Moreover, Fourier transform infrared spectroscopy studies have shown that phosphorus in non-phosphated layers of ferromanganese crusts is mainly found in the form of phosphate ions (PO_4^{3-}) [62]. Manganese oxides have a negative surface charge (fraction II) and preferentially sequester the monocarbonate form of neodymium $(NdCO_3^+)$. The revealed influence of meltwater with a more negative ε_{Nd} value on the formation of the isotopic composition of seawater in the northern Pacific confirms that the isotopic composition of seawater is mainly determined by terrigenous inputs [27,63].

Additionally, the percentage of neodymium bound to hydrous Fe oxides in samples with decreased ε_{Nd} values is high (Figure 6). This REEs distribution between Mn and Fe oxides is attributed to the influence of hydrothermal matter and has been observed in the crusts in a mixed hydrogenous–hydrothermal genesis. In hydrogenetic deposits, similar REEs between these two fractions were observed [25]. In our case, the high REE content

in the Fe oxide fraction relative to the Mn fraction suggests additional sorption of REE phosphate complexes in ferrous oxyhydroxides.

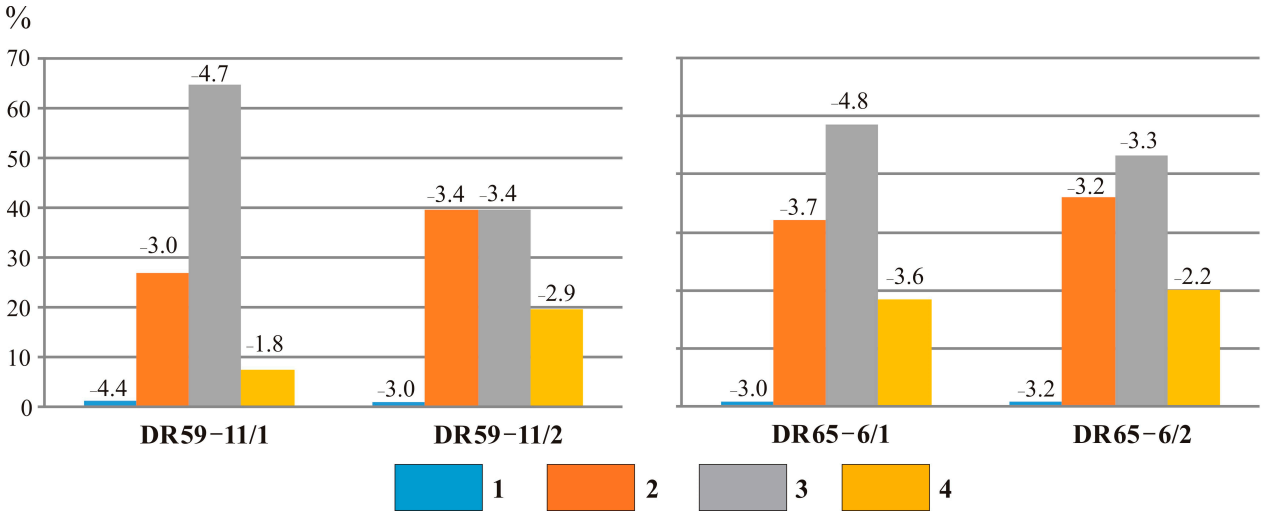

Figure 6. Histograms of ε_{Nd} value in different mineral fractions. 1—loosely bound; 2—Mn oxides; 3—hydrous Fe oxides; 4—residual.

Furthermore, we observed a linear relationship between ε_{Nd} values and $^{87}Sr/^{86}Sr$ ratios (Figure 7). This indicates a single source of detrital materials with similar initial isotope-geochemical characteristics during the depositional period.

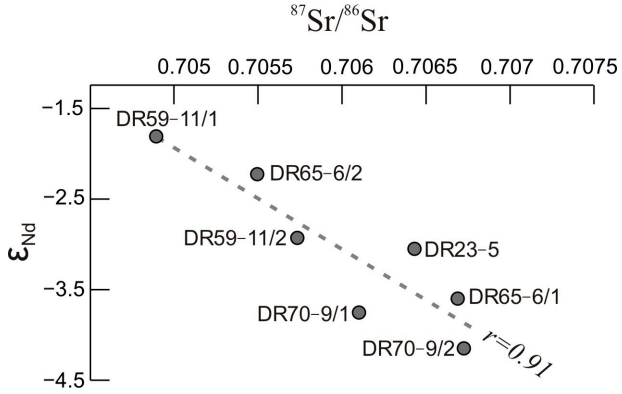

Figure 7. Scatter plot of ε_{Nd} value vs. $^{87}Sr/^{86}Sr$ ratio in residual fraction of ferromanganese crusts.

Terrigenous matters in these crusts in our study are primarily delivered through the Strait of Kamchatka. Over the past 40 Myr, the Meiji Drift has formed in the southern tip of this strait, situated between the Emperor Ridge and the Aleutian Island Arc [31]. The main sediment sources in this area are from the Yukon, Kuskokwim, and Anadyr Rivers, as well as rivers from Kamchatka flowing into the Bering Sea [64]. The $^{87}Sr/^{86}Sr$ ratio and ε_{Nd} values of these rocks vary considerably, ranging from 0.703 to 0.709 and from −10.1 to +9, respectively [20,65]. The $^{87}Sr/^{86}Sr$ ratio in the residual fraction of the studied samples varies from 0.705 to 0.706 (Table 3), generally agreeing with the average value of weathered rocks in the Bering Sea pool. Aeolian material is not a significant proportion [28], because the rates of dust deposition are low [66], only about an order lower than the one near the Meiji Drift [31].

Fine sediments in the Meiji Drift (ODP Hole 884) reveals that the rocks are dated to 40–60 Ma, with ε_{Nd} values of −1 to +2 during glacial periods, while during interglacial periods, younger rocks (2–15 Ma) have much higher ε_{Nd} values, from +5 to +9 [64]. Therefore, an increase in ε_{Nd} values in the silicate fraction of the studied crusts in the northernmost

Pacific may indicate a higher concentration of eroded materials from young island arc rocks during warming periods. An increase in the supply of drop stones during the warming period was detected in the upper part of the DR65-6 sample during elemental scanning, expressed in a high content of Si and Al (Figure 8, [67]).

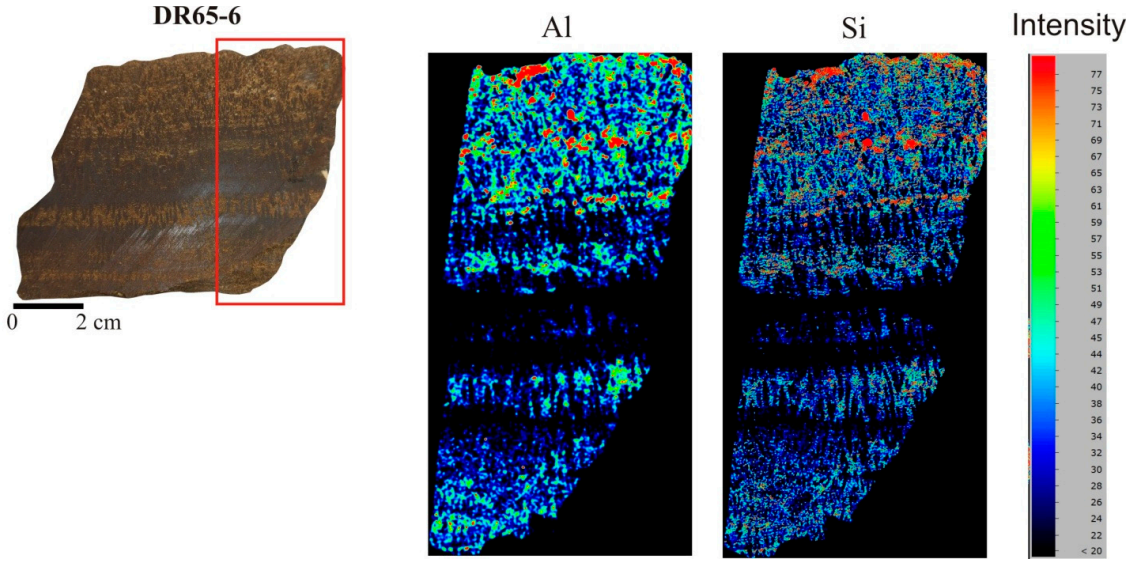

Figure 8. Element distribution of the studied part of the DR65-6 sample. Red frame is studied area.

5. Conclusions

We studied the isotopic composition of neodymium and strontium in four mineral fractions of the hydrogenous ferromanganese crusts of the northernmost Pacific in this work.

The $^{87}Sr/^{86}Sr$ ratios of chemogenic fractions (I, II, III) are similar (0.70913 ± 0.00010), close to the ratio in contemporary ocean water (0.70917). This supports the assumption that the exchange and mixing of the strontium isotopic composition takes place between seawater and the crust. Therefore, the data obtained from the ferromanganese crusts cannot be used for the Sr isotopic stratigraphy.

The decreased ε_{Nd} value in the ferrous (III) fraction seems to be related to the presence of REE phosphate complexes in seawater. The increase in those complexes is a consequence of melt waters during warming periods, which have a more negative ε_{Nd} value.

Our studies show that the carbonate REE complexes are not the dominant form, which leads to ε_{Nd} differences in the manganese and ferrous fractions of hydrogenous ferromanganese crusts. A decrease in the ε_{Nd} value in the ferrous fraction relative to the manganese fraction may indicate a local increase in surface water bioproductivity. Moreover, our data show that the increased REE in the ferrous fraction does not reflect the influence of hydrothermal materials, as shown for the ferromanganese deposits in the mid-ocean ridges in the Indian Ocean [25].

Based on isotopic (Sr, Nd) characteristics, the detrital matters in ferromanganese crusts has a common source with the Meiji Drift sediments.

Author Contributions: Conceptualization, P.M., I.V. and L.Y.; methodology, I.V. and N.S.; software, P.M., N.S. and V.P.; formal analysis, I.V. and N.S.; investigation, P.M.; resources, P.M. and V.P.; data curation, I.V.; writing—original draft preparation, P.M., I.V. and L.Y.; writing—review and editing, P.M. and L.Y.; visualization, P.M. and I.V.; supervision, P.M.; project administration, P.M.; funding acquisition, P.M. and V.P. All authors have read and agreed to the published version of the manuscript.

Funding: This research was undertaken thanks to Grant No. 22-27-00079 from the Russian Science Foundation, https://rscf.ru/en/project/22-27-00079/ (accessed on 21 June 2022).

Institutional Review Board Statement: Not applicable.

Informed Consent Statement: Not applicable.

Data Availability Statement: All data have been provided in the paper.

Acknowledgments: The authors are grateful to M.V. Portnyagin and D.P. Saveliev for donating ferromanganese crusts for the study, which were dredged during the scientific expedition of the marine research ship "Sonne" (249th cruise, 2016) of the BERING project, the expedition having been sponsored by the German Ministry of Education and Research.

Conflicts of Interest: The authors declare that the research was conducted in the absence of any commercial or financial relationships that could be construed as potential conflicts of interest. Any use of trade, product, or firm names is for descriptive purposes only and does not imply endorsement by the authors or their affiliated institutions.

References

1. Halbach, P.E.; Jahn, A.; Cherkashov, G. Marine Co-Rich Ferromanganese Crust Deposits: Description and Formation, Occurrences and Distribution, Estimated World-wide Resources. In *Deep-Sea Mining: Resource Potential, Technical and Environmental Considerations*; Sharma, R., Ed.; Springer International Publishing: Cham, Switzerland, 2017; pp. 65–141. [CrossRef]
2. Hein, J.R.; Koschinsky, A.; Kuhn, T. Deep-ocean polymetallic nodules as a resource for critical materials. *Nat. Rev. Earth Environ.* **2020**, *1*, 158–169. [CrossRef]
3. Yi, L.; Medina-Elizalde, M.; Tan, L.; Kemp, D.B.; Li, Y.; Kletetschka, G.; Xie, Q.; Yao, H.; He, H.; Deng, C.; et al. Plio-Pleistocene deep-sea ventilation in the Eastern Pacific and potential linkages with Northern Hemisphere glaciation. *Sci. Adv.* **2023**, *9*, eadd1467. [CrossRef] [PubMed]
4. Koschinsky, A.; Hein, J.R. Marine Ferromanganese Encrustations: Archives of Changing Oceans. *Elements* **2017**, *13*, 177–182. [CrossRef]
5. Toro, N.; Robles, P.; Jeldres, R.I. Seabed mineral resources, an alternative for the future of renewable energy: A critical review. *Ore Geol. Rev.* **2020**, *126*, 103699. [CrossRef]
6. Bonatti, E.; Kreamer, T.; Rydell, H. *Classification and Genesis of Submarine Iron Manganese Deposits. Ferromanganese Deposits on the Ocean Floor: Office for the International Decade of Ocean Exploration*; National Science Foundation: Washington, DC, USA, 1972; pp. 149–165.
7. Hein, J.R.; Koschinsky, A. 13.11—Deep-Ocean Ferromanganese Crusts and Nodules. In *Treatise on Geochemistry*, 2nd ed.; Holland, H., Turekian, K., Eds.; Elsevier: Amsterdam, The Netherlands, 2014; pp. 273–291. [CrossRef]
8. Mikhailik, P.E.; Vishnevskaya, I.A.; Mikhailik, E.V.; Blokhin, M.G.; Chervyakovskaya, M.V.; Rashidov, V.A.; Ren, X. Genesis and Nd Isotope Composition of Ferromanganese Deposits of the Sea of Okhotsk and the Kuril Island Arc. *Russ. Geol. Geophys.* **2021**, *62*, 1074–1087. [CrossRef]
9. Mikhailik, P.E.; Vishnevskaya, I.A.; Mikhailik, E.V.; Rashidov, V.A.; Savelyev, D.P.; Soloshenko, N.G. Srand Nd isotopes in hydrogenetic ferromanganese crusts from the North Pacific. *Bull. Tomsk Polytech. Univ. Geo Assets Eng.* **2023**, *334*, 7–21. [CrossRef]
10. Manheim, F.T.; Lane-Bostwick, C.M. Cobalt in ferromanganese crusts as a monitor of hydrothermal discharge on the sea floor. *Nature* **1988**, *335*, 59–62. [CrossRef]
11. Scher, H.D.; Martin, E.E. Circulation in the Southern Ocean during the Paleogene inferred from neodymium isotopes. *Earth Planet. Sci. Lett.* **2004**, *228*, 391–405. [CrossRef]
12. Jones, K.M.; Khatiwala, S.P.; Goldstein, S.L.; Hemming, S.R.; van de Flierdt, T. Modeling the distribution of Nd isotopes in the oceans using an ocean general circulation model. *Earth Planet. Sci. Lett.* **2008**, *272*, 610–619. [CrossRef]
13. Siddall, M.; Khatiwala, S.; van de Flierdt, T.; Jones, K.; Goldstein, S.L.; Hemming, S.; Anderson, R.F. Towards explaining the Nd paradox using reversible scavenging in an ocean general circulation model. *Earth Planet. Sci. Lett.* **2008**, *274*, 448–461. [CrossRef]
14. Carter, P.; Vance, D.; Hillenbrand, C.D.; Smith, J.A.; Shoosmith, D.R. The neodymium isotopic composition of waters masses in the eastern Pacific sector of the Southern Ocean. *Geochim. Et Cosmochim. Acta* **2012**, *79*, 41–59. [CrossRef]
15. Williams, T.J.; Martin, E.E.; Sikes, E.; Starr, A.; Umling, N.E.; Glaubke, R. Neodymium isotope evidence for coupled Southern Ocean circulation and Antarctic climate throughout the last 118,000 years. *Quat. Sci. Rev.* **2021**, *260*, 106915. [CrossRef]
16. Frank, M. Radiogenic isotopes: Tracers of past ocean circulation and erosional input. *Rev. Geophys.* **2002**, *40*, 1–38. [CrossRef]
17. Jeandel, C.; Arsouze, T.; Lacan, F.; Téchiné, P.; Dutay, J.-C. Isotopic Nd compositions and concentrations of the lithogenic inputs into the ocean: A compilation, with an emphasis on the margins. *Chem. Geol.* **2007**, *239*, 156–164. [CrossRef]
18. Burton, K.W.; Vance, D. Glacial–interglacial variations in the neodymium isotope composition of seawater in the Bay of Bengal recorded by planktonic foraminifera. *Earth Planet. Sci. Lett.* **2000**, *176*, 425–441. [CrossRef]
19. Piotrowski, A.M.; Goldstein, S.L.; Hemming, S.R.; Fairbanks, R.G. Temporal relationships of carbon cycling and ocean circulation at glacial boundaries. *Science* **2005**, *307*, 1933–1938. [CrossRef]
20. Horikawa, K.; Asahara, Y.; Yamamoto, K.; Okazaki, Y. Intermediate water formation in the Bering Sea during glacial periods: Evidence from neodymium isotope ratios. *Geology* **2010**, *38*, 435–438. [CrossRef]
21. Roberts, N.L.; Piotrowski, A.M.; McManus, J.F.; Keigwin, L.D. Synchronous deglacial overturning and water mass source changes. *Science* **2010**, *327*, 75–78. [CrossRef]

22. Chen, T.; Zheng, J.; Li, T.; Shi, X.; Robinson, L.F.; Wang, M.; Li, G.; Ling, H.; Ren, X.; Ji, J. Thorium isotope evidence for glacial–interglacial dust storminess and productivity in the North Pacific gyre. *Geochim. Et Cosmochim. Acta* **2023**, *346*, 15–28. [CrossRef]
23. Prakash, S.L.; Ray, D.; Paropkari, A.L.; Mudholkar, A.V.; Satyanarayanan, M.; Sreenivas, B.; Chandrasekharam, D.; Kota, D.; Kamesh Raju, K.A.; Kaisary, S.; et al. Distribution of REEs andyttrium among major geochemical phases of marine Fe–Mn-oxides: Comparative study between hydrogenous and hydrothermal deposits. *Chem. Geol.* **2012**, *312*, 127–137. [CrossRef]
24. Mikhailik, P.E.; Mikhailik, E.V.; Zarubina, N.V.; Blokhin, M.G. Distribution of rare-earth elements and yttrium in hydrothermal sedimentary ferromanganese crusts of the Sea of Japan (from phase analysis results). *Russ. Geol. Geophys.* **2017**, *58*, 1530–1542. [CrossRef]
25. Prakash, S.L.; Ray, D.; Nagender Nath, B.; Satyanarayanan, M.; Kamesh Raju, K.A.; Kurian, J.P.; Dileep Kumar, M.; Srinivas Rao, A. Anomalous phase association of REE in ferromanganese crusts from Indian mid-oceanic ridges: Evidence for large scale dispersion of hydrothermal iron. *Chem. Geol.* **2020**, *549*, 119679. [CrossRef]
26. Frank, M.; O'Nions, R.K.; Hein, J.R.; Banakar, V.K. 60 Myr records of major elements and Pb–Nd isotopes from hydrogenous ferromanganese crusts: Reconstruction of seawater paleochemistry. *Geochim. Et Cosmochim. Acta* **1999**, *63*, 1689–1708. [CrossRef]
27. Ren, J.; He, G.; Deng, X.; Deng, X.; Yang, Y.; Yao, H.; Yang, S. Metallogenesis of Co-rich ferromanganese nodules in the northwestern Pacific: Selective enrichment of metallic elements from seawater. *Ore Geol. Rev.* **2022**, *143*, 104778. [CrossRef]
28. van de Flierdt, T.; Frank, M.; Lee, D.-C.; Halliday, A.N.; Reynolds, B.C.; Hein, J.R. New constraints on the sources and behavior of neodymium and hafnium in seawater from Pacific Ocean ferromanganese crusts. *Geochim. Et Cosmochim. Acta* **2004**, *68*, 3827–3843. [CrossRef]
29. Hyeong, K.; Kuroda, J.; Seo, I.; Wilson, P.A. Response of the Pacific inter-tropical convergence zone to global cooling and initiation of Antarctic glaciation across the Eocene Oligocene Transition. *Sci. Rep.* **2016**, *6*, 30647. [CrossRef]
30. Clague, D.A.; Dalrymple, G.B. The Hawaiian-Emperor volcanic chain. part I. Geologic evolution. *Volcanism Hawaii* **1987**, *1*, 5–54. Available online: https://hdl.handle.net/10524/33604 (accessed on 5 January 2021).
31. Rea, D.K.; Basov, L.A.; Scholl, D.W.; Allan, J.F. (Eds.) *Proceedings ODP, Science Results*; Ocean Drilling Program: College Station, TX, USA, 1995; Volume 145, p. 690. [CrossRef]
32. Tarduno, J.A.; Duncan, R.A.; Scholl, D.W.; Cottrell, R.D.; Steinberger, B.; Thordarson, T.; Kerr, B.C.; Neal, C.R.; Frey, F.A.; Torii, M.; et al. The Emperor Seamounts: Southward Motion of the Hawaiian Hotspot Plume in Earth's Mantle. *Science* **2003**, *301*, 1064. [CrossRef]
33. Sun, W.; Langmuir, C.H.; Ribe, N.M.; Zhang, L.; Sun, S.; Li, H.; Li, C.; Fan, W.; Tackley, P.J.; Sanan, P. Plume-ridge interaction induced migration of the Hawaiian-Emperor seamounts. *Sci. Bull.* **2021**, *66*, 1691–1697. [CrossRef]
34. Hoernel, K.; Jicha, B.R.; Müller, D.; Portnyagin, M.; Werner, R.; Hauff, F.; Bezard, R.; Höfig, T.W.; Yogodzinski, G. *Role of the Aleutian Arc and NW Pacific Seafloor in Pacific—Wide Plate Reorganization in the Paleogene*; American Geophysical Union: Washington, DC, USA, 2019; Fall Meeting, 2019, #T51A-02.
35. Werner, R.; Hoernle, K.; Hauff, F.; Portnyagin, M.; Yogodzinsky, G.; Ziegler, A. (Eds.) *RV SONNE Fahrtbericht/Cruise Report SO249 BERING–Origin and Evolution of the Bering Sea: An Integrated Geochronological, Volcanological, Petrological and Geochemical Approach, Leg 1: Dutch Harbor (U.S.A.)-Petropavlovsk-Kamchatsky (Russia), 05.06.2016–15.07.2016, Leg 2: Petropavlovsk-Kamchatsky (Russia)-Tomakomai (Japan), 16.07.2016–14.08.2016. Geomar Report, N. Ser. 030*; Geomar Helmholtz-Zentrum fьr Ozeanforschung: Kiel, Germany, 2016; p. 451.
36. Mikhailik, P.E.; Khanchuk, A.I.; Mikhailik, E.V.; Rashidov, V.A.; Savelev, D.P.; Zarubina, N.V. Ferromanganese Crusts of the North Pacific Ocean. *Russ. J. Pac. Geol.* **2023**, *17*, 101–133. [CrossRef]
37. Hein, J.R.; Mizell, K.; Koschinsky, A.; Conrad, T.A. Deep-ocean mineral deposits as a source of critical metals for high- and green-technology applications: Comparison with land-based resources. *Ore Geol. Rev.* **2013**, *51*, 1–14. [CrossRef]
38. McLennan, S.M. Rare earth elements in sedimentary rocks: Influence of provenance and sedimentary processes. In *Geochemistry and Mineralogy of the Rare Earth Elements. Review Mineralogy*; Lipin, B.R., McKay, G.A., Eds.; De Gruyter: Berlin, Germany, 1989; Volume 21, pp. 169–200.
39. Bau, M.; Schmidt, K.; Koschinsky, A.; Hein, J.R.; Kuhn, T.; Usui, A. Discriminating between different genetic types of marine ferro-manganese crusts and nodules based on rare earth elements and yttrium. *Chem. Geol.* **2014**, *381*, 1–9. [CrossRef]
40. Koschinsky, A.; Hein, J.R. Uptake of elements from seawater by ferromanganese crusts: Solid phase associations and seawater speciation. *Mar. Geol.* **2003**, *198*, 331–351. [CrossRef]
41. Jacobsen, S.B.; Wasserburg, G.J. Sm-Nd isotopic evolution of chondrites. *Earth Planet. Sci. Lett.* **1980**, *50*, 139–155. [CrossRef]
42. Piepgras, D.J.; Jacobsen, S.B. The isotopic composition of neodymium in the North Pacific. *Geochim. Et Cosmochim. Acta* **1988**, *52*, 1373–1381. [CrossRef]
43. Ling, H.F.; Burton, K.W.; O'nions, R.K.; Kamber, B.S.; von Bla, N.F.; Gibb, A.J.; Hein, J.R. Evolution of Nd and Pb isotopes in Central Pacific seawater from ferromanganese crusts. *Earth Planet. Sci. Lett.* **1997**, *146*, 1–12. [CrossRef]
44. McArthur, J.M.; Howarth, R.J.; Shields, G.A.; Zhou, Y. Chapter 7. Strontium isotope stratigraphy. In *Geologic Time Scale*; Gradstein, F., Ogg, G., Schmitz, D., Ogg, M., Eds.; Elsevier: Amsterdam, The Netherland, 2020; pp. 211–238. [CrossRef]
45. Henderson, G.M.; Burton, K.W. Using ($^{234}U/^{238}U$) to Assess Diffusion Rates of Isotope Tracers in Ferromanganese Crusts. *Earth Planet. Sci. Lett.* **1999**, *70*, 169–179. [CrossRef]

46. Gutjahr, M.; Frank, M.; Stirling, C.H.; Klemm, V.; van de Flierdt, T.; Halliday, A.N. Reliable extraction of a deepwater trace metal isotope signal from Fe–Mn oxyhydroxide coatings of marine sediments. *Chem. Geol.* **2007**, *242*, 351–370. [CrossRef]
47. Khanchuk, A.I.; Mikhailik, P.E.; Mikhailik, E.V.; Zarubina, N.V.; Blokhin, M.G. Peculiarities of the Distribution of Rare Earth Elements and Yttrium in Mineral Phases of the Ferromanganese Crusts from the Detroit Guyot (Pacific Ocean). *Dokl. Earth Sci.* **2015**, *465*, 1243–1247. [CrossRef]
48. Bau, M.; Koschinsky, A. Oxidative scavenging of cerium on hydrous Fe oxide: Evidence from the distribution of rare earth elements and yttrium between Fe oxides and Mn oxides in hydrogenetic ferromanganese crusts. *Geochem. J.* **2009**, *43*, 37–47. [CrossRef]
49. Jiang, X.; Lin, X.; Yao, D.; Guo, W. Enrichment mechanisms of rare earth elements in marine hydrogenic ferromanganese crusts. *Sci. China Earth Sci.* **2011**, *54*, 197–203. [CrossRef]
50. Conrad, T.A.; Nielsen, S.G.; Peucker-Ehrenbrink, B.; Blusztajn, J.; Winslow, D.; Hein, J.R.; Paytan, A. Reconstructing the evolution of the submarine Monterey Canyon System from Os, Nd, and Pb isotopes in hydrogenetic Fe-Mn crusts. *Geochem. Geophys. Geosystems* **2017**, *18*, 3946–3963. [CrossRef]
51. Benn, D.I.; Evans, D.J.A. *Glaciers & Glaciation*; Routledge: Abingdon, UK, 2014.
52. Ruttenberg, K.C. The global phosphorus cycle. *Treatise Geochem.* **2003**, *8*, 682. [CrossRef]
53. Sancetta, C.; Robinson, S.W. Diatom evidence on Wisconsin and Holocene events in the Bering Sea. *Quat. Res.* **1983**, *20*, 232–245. [CrossRef]
54. Tanaka, S.; Takahashi, K. Late Quaternary paleoceanographic changes in the Bering Sea and the western subarctic Pacific based on radiolarian assemblages. *Deep. Sea Res. Part II Top. Stud. Oceanogr.* **2005**, *52*, 2131–2149. [CrossRef]
55. Smirnova, M.A.; Kazarina, G.K.; Matul, A.G.; Max, L. Diatom evidence for paleoclimate changes in the northwestern Pacific during the last 20000 years. *Oceanology* **2015**, *55*, 383–389. [CrossRef]
56. Horikawa, K.; Martin, E.E.; Asahara, Y.; Sagawa, T. Limits on conservative behavior of Nd isotopes in seawater assessed from analysis of fish teeth from Pacific core tops. *Earth Planet. Sci. Lett.* **2011**, *310*, 119–130. [CrossRef]
57. Hu, R.; Piotrowski, A.M.; Bostock, H.C.; Crowhurst, S.; Rennie, V. Variability of neodymium isotopes associated with planktonic foraminifera in the Pacific Ocean during the Holocene and Last Glacial Maximum. *Earth Planet. Sci. Lett.* **2016**, *447*, 130–138. [CrossRef]
58. Koschinsky, A.; Halbach, P. Sequential leaching of marine ferromanganese precipitates: Genetic implications. *Geochim. Et Cosmochim. Acta* **1995**, *59*, 5113–5132. [CrossRef]
59. Johanneson, K.H.; Lyons, W.B.; Stetzenbach, K.J.; Byrne, R.H. The solubility control of rare earth elements in natural terrestrial waters and the significance of PO_4^{3-} and CO_3^{2-} in limiting dissolved rare earth concentrations: A review of recent information. *Aquat. Geochem.* **1995**, *1*, 157–173. [CrossRef]
60. Dubinin, A.V. *Geochemistry of Oceanic Rare-Earth Elements*; Volkov, I.I., Ed.; Nauka: Moscow, Russia, 2006; 360p, ISBN 5-02-033745-5. (In Russian)
61. Byrne, R.H. Inorganic speciation of dissolved elements in seawater: The influence of pH on concentration ratios. *Geochem. Trans.* **2002**, *3*, 11–16. [CrossRef] [PubMed]
62. Zhou, J.; Yang, S.; Cao, J.; Deng, Y.; Wei, Z.; Li, Y.; Tian, D.; Hu, G. Influence of Phosphatization in REY Geochemistry in Ferromanganese Crusts in Line Islands, Central Pacific. *Minerals* **2023**, *13*, 647. [CrossRef]
63. Zhao, K.D.; Jiang, S.Y.; Zheng, X.Y.; Chen, T.Y.; Ling, H.F. Nd isotope evolution of ocean waters and implications for paleo-ocean circulation. *Earth Sci. Front.* **2009**, *16*, 160–171, (In Chinese with English abstract).
64. VanLaningham, S.; Pisias, N.G.; Duncan, R.A.; Clift, P.D. Glacial–interglacial sediment transport to the Meiji Drift, northwest Pacific Ocean: Evidence for timing of Beringian outwashing. *Earth Planet. Sci. Lett.* **2009**, *277*, 64–72. [CrossRef]
65. Jang, K.; Huh, Y.; Han, Y. Diagenetic overprint on authigenic Nd isotope records: A case study of the Bering Slope. *Earth Planet. Sci. Lett.* **2018**, *498*, 247–256. [CrossRef]
66. Pettke, T.; Halliday, A.N.; Hall, C.M.; Rea, D.K. Dust production and deposition in Asia and the north Pacific Ocean over the past 12 Myr. *Earth Planet. Sci. Lett.* **2000**, *178*, 397–413. [CrossRef]
67. Yi, L.; Li, Y.; Mikhailik, P.; Qi, Y.; Deng, C. Magnetic and geochemical scanning reveals growth history of marine ferromanganese crust on Detroit Seamount, Northwest Pacific since the Early Miocene. *Quat. Int.* 2023, *in press*. [CrossRef]

Disclaimer/Publisher's Note: The statements, opinions and data contained in all publications are solely those of the individual author(s) and contributor(s) and not of MDPI and/or the editor(s). MDPI and/or the editor(s) disclaim responsibility for any injury to people or property resulting from any ideas, methods, instructions or products referred to in the content.